Monte Carlo simulations of copolymers at homopolymer interfaces: Interfacial structure as a function of the copolymer density

3 AUTHORS, INCLUDING:

Friederike Schmid
Johannes Gutenberg-Universität Mainz
155 PUBLICATIONS 2,569 CITATIONS

SEE PROFILE

Marcus Müller
Georg-August-Universität Göttingen
340 PUBLICATIONS 10,220 CITATIONS

SEE PROFILE

Monte Carlo simulations of copolymers at homopolymer interfaces: Interfacial structure as a function of the copolymer density

A. Werner, F. Schmid, M. Müller

Institut für Physik, Universität Mainz, D-55099 Mainz, Germany

Abstract. By means of extensive Monte Carlo simulations of the bond fluctuation model, we study the effect of adding AB diblock copolymers on the properties of an interface between demixed homopolymer phases. The parameters are chosen such that the homopolymers are strongly segregated, and the whole range of copolymer concentrations in the two phase coexistence region is scanned. We compare the "mushroom" regime, in which copolymers are diluted and do not interact with each other, with the "wet brush" regime, where copolymers overlap and stretch, but are still swollen by the homopolymers. A "dry brush" regime is never entered for our choice of chain lengths. "Intrinsic" profiles are calculated using a block analysis method introduced by us in earlier work. We discuss density profiles, orientational profiles and contact number profiles. In general, the features of the profiles are similar at all copolymer concentrations, however, the profiles in the concentrated regime are much broader than in the dilute regime. The results compare well with self-consistent field calculations.

I. INTRODUCTION

Polymers of different types are usually immiscible [1,2]. When blending different polymers together, one often obtains a mesoscopically structured material which contains numerous droplets of one phase finely dispersed in the other. The structure of the interfaces between the two phases, as well as the number and size of the droplets thus crucially determine the properties of the composite material. The droplet size, in turn, depends not only on the conditions of preparation and kinetic factors, but also on the interfacial tension [3,4].

Understanding the interfacial properties and, if possible, improving them has therefore been a matter of longstanding interest [5,6]. Interfacial properties can be tuned in a very efficient way by adding surfactants which adsorb at the interface. In the case of homopolymer blends, the most natural surfactant molecules are copolymers, in which monomers of both types are connected to each other by chemical links [7–9].

The effect of copolymers on homopolymer interfaces is twofold. First, they reduce the number of direct contacts between homopolymers, thereby reducing the interfacial tension [10–17]. Second, they significantly enlarge the interfacial region, where polymers bridging the interface between the coexisting phases can entangle, thereby increasing the fracture toughness [18,19]. Note that in pure homopolymer interfaces, the entanglements which contribute to the mechanical stability are those between polymers of different type, and are thus confined to the narrow region where A and B polymers actually come into contact. If

1

copolymers come into play, the relevant entanglements are those between adsorbed copolymers and homopolymers, which are located in a region with a width determined by the copolymer radius of gyration.

The energetic factors which favor the adsorption of copolymers at interfaces are balanced against two opposing entropic factors: The loss of translational entropy of copolymers and homopolymers, and at higher copolymer densities the elastic energy of stretching of the copolymer blocks. Following Leibler and Semenov [10,11], one can distinguish between four different regimes: At very low copolymer concentrations (mushroom regime), the copolymers adsorb at the interface, arrange themselves such that each block sticks into its majority phase, and do not interact with each other. As the copolymer concentration increases, the different blocks start to overlap and the system enters the wet brush regime, where copolymers are forced to stretch, but remain swollen by the homopolymers. In the dry brush regime at even higher copolymer concentrations, the homopolymers are completely expelled from the central interfacial region. Finally, in the last regime, the interface cannot accommodate any additional copolymers and saturates.

On increasing the chemical potential of the copolymers, the excess concentration of copolymers at the interface increases and one should thus pass through these different regimes. However, the process is usually interrupted at some point due to the formation of a new, copolymer-rich phase [14,20–22]. This phase can be either ordered [21,22] or disordered but structured, *i.e.*, a microemulsion [23–25]. This has been also observed by experiments of Balsara [25] and co-workers and Bates *et al* [24].

The structure of copolymers at interfaces has been studied intensely in experiments [13,16,26–36], and theoretically by various refined mean field theories [37–41]. Computer simulations provide a useful way of obtaining additional structural information, and testing theoretical concepts [42]. Being computationally very demanding, only very few studies of homopolymer interfaces in the presence of copolymers exist so far [23,43–48].

In our earlier work [47], we have studied by Monte Carlo simulation the structure of symmetric diblock (AB) copolymers at a homopolymer (A/B) interface in the highly dilute mushroom regime within the bond fluctuation model (see section II). Our main results can be summarized as follows: The copolymers in this non–overlapping regime assume the shape of oriented dumbbells. The conformations of the individual blocks resemble on average those of hardly perturbed homopolymer coils. In particular, single blocks tend to show preferential alignment parallel to the interface, even though the copolymers as a whole orient perpendicular to the interface. Second, copolymers were found to be significantly more compact than homopolymers at the center of the interface, *i.e.*, they have more intrachain contacts and fewer interchain contacts. At distances of a few radii of gyration from the interface, on the other hand, the opposite trend is found: the number of interchain contacts increases at the expense of the self contacts. In the present paper, we extend our previous work to the study of interfaces with higher copolymer content.

The bulk phase behavior of ternary mixtures of A,B homopolymers and symmetric (AB) diblock copolymers has been investigated in detail by one of us [23]. Fig. 1 summarizes the resulting phase diagram (see section II for a description of the simulation model). The addition of small amounts of copolymers has the effect of shifting the unmixing transition towards higher incompatibilities χ. At higher copolymer concentration, a tricritical point is encountered and a miscibility gap opens up in which a copolymer rich phase, either a microemulsion or at large χN a lamellar phase, coexists with an A-rich or B-rich phase. The

interfacial tension of the A/B interface was extracted by histogram reweighting methods, and the Fourier spectrum of capillary waves of an interface at moderate incompatibility ($\chi N = 9.2$) was analyzed in order to obtain some information on the bending stiffness. It was found to be very small, $\kappa/k_B T < 0.08$.

Here, we shall study the structure of the interface in microscopic detail, for the case of strong segregation ($\chi N = 17.3$) and for copolymer concentrations spanning the whole range from the dilute limit to the point where phase separation sets in. Note that the coexisting copolymer rich phase here is lamellar. As in our previous work [47], we shall focus on local properties, on profiles of local contacts and chain orientations, and local density profiles. We will compare the structure of the interface in the mushroom regime and in the wet brush regime. The dry brush regime is never reached, as we shall see: The homopolymers swell the copolymers throughout the interface at all concentrations.

In order to establish this last result in particular, it is necessary to separate the local, intrinsic profiles from the capillary waves of the interfacial position. This is done *via* a block analysis procedure, which we have already applied successfully to the study of homopolymer interfaces [49–51]. As far as possible, the results will be compared to the predictions of a Helfand type self-consistent field theory [37,40,52,53].

Our paper is organized as follows: In section II, we describe the simulation model and the method and characterize the system in somewhat more detail. The results are presented in section III. First, we discuss the interfacial width and the interfacial tension. Then, we study the effect of copolymer crowding on the contact number profiles and the orientational properties. We summarize and conclude in section IV.

II. MODEL AND TECHNICAL DETAILS

As in our earlier work, we use the bond fluctuation model, which is a lattice model for polymer chains [54]. Three to five chemical repeat units are mapped onto one "effective" monomer, which occupies a cube of eight lattice sites on a simple cubic lattice. Monomers are connected by bonds of variable length 2, $\sqrt{5}$, $\sqrt{6}$, 3, or $\sqrt{10}$. We work at the filling fraction 1/2, or monomer number density $\rho_b = 1/16$, at which single chain configuration show almost ideal Gaussian chain statistics, *i.e.*, properties of a dense polymer melt are recovered [55]. The chain length is chosen as in Refs. [23,47], $N = 32$. The chains then have the radius of gyration $R_g = b\sqrt{(N-1)/6} = 6.96$ with the statistical segment length $b = 3.06$ in units of the lattice constants.

To distinguish between monomers A and B, we introduce an interaction potential acting between monomers with a distance of less or equal $\sqrt{6}$ lattice constants: $\epsilon_{AA} = \epsilon_{BB} = -\epsilon_{AB} = k_B T \epsilon$. The parameter ϵ thus determines the relative repulsion of unlike monomers. Here we use $\epsilon = 0.1$, which is well in the regime where homopolymers demix ($\epsilon_c = 0.014$ [56]). From ϵ one can estimate the Flory-Huggins parameter χ by [57]

$$\chi = 2z_{\text{eff}}\epsilon, \tag{1}$$

where z_{eff} is the average number of interchain contacts of a monomer. In our case, we measure $z_{\text{eff}} = 2.71$ in the demixed homopolymer bulk phase, which leads to $\chi = 0.54$.

We study ternary mixtures of A and B homopolymers and symmetric AB diblock copolymers in the canonical and in the semi-grandcanonical ensemble. In the latter, the total

number of polymers remains constant, but the polymers can switch their identity between A or B homopolymer and copolymer. The composition is then driven by two independent combinations of the chemical potentials [23].

$$\Delta\mu = \mu_A - \mu_B \qquad \text{and} \qquad \delta\mu = \mu_C - \frac{1}{2}(\mu_A + \mu_B), \qquad (2)$$

where μ_A and μ_B are the chemical potential of the homopolymers , and μ_C denotes the copolymer potential. Two phase coexistence between an A rich and a B rich phase is found at $\Delta\mu = 0$. The other variable $\delta\mu$ determines the copolymer concentration.

In order to enforce a well-defined interface between an A-rich and a B-rich phase, we place the system in a thick film of thickness D between asymmetric walls, one of which favors A and the other B. The wall potentials $\epsilon_w = 0.1$ act on monomers in the first two layers next to the wall, and are chosen strong enough that each component wets its corresponding wall. Therefore, the interface is located on average in the middle of the film. In the lateral dimension L, periodic boundary conditions are applied. Specifically, we use $L = 128$ and $D = 64$ or $D = 128$, which ensures that the film is thick enough that the interfacial properties are not affected by the walls [49]. The system is equilibrated in the semi-grandcanonical ensemble. The Monte Carlo moves include single monomer hopping moves, slithering snake moves [58], identity switches of polymers, and polymer exchanges. After 2×10^6 Monte Carlo steps (MCS) which is well after the correct bulk concentrations of homopolymers and copolymers have been reached in the wings of the profiles, we turn off the identity switches and start to collect data. Here four Monte Carlo steps correspond to one local hopping attempt per monomer, three slithering snakes trials per chain and 0.1 canonical particle exchange moves. Our results thus refer to the canonical ensemble. The samples include every 5000st configuration in runs of total length 2×10^6 MCS, *i.e.*, 400 configurations.

"Intrinsic profiles" profiles are obtained by a block analysis which we have already applied successfully to homopolymer interfaces [49–51]. The system is divided into blocks of size $B \times B \times D$ and the interface position $h(x, y)$ is determined in each block. This allows to study the capillary waves of the interface position $h(x, y)$ (see section 3.1) and to average over local profiles relative to the local interface position. We shall use the block size $B = 8$ which was found to be a suitable choice at $N = 32$ and $\epsilon = 0.1$ in our earlier studies (see Ref. [51] for a detailed discusstion of this "intrinsic coarse graining length").

Our results are compared to self-consistent field calculations [52,59]. Polymers are described as continuous space curves $\vec{r}(s)$, $s \in [0 : N]$ with statistical weight

$$\mathcal{P}\{\vec{r}(\cdot)\} = \mathcal{N} \exp\left[-\frac{3}{2b^2} \int_0^N ds \left|\frac{d\vec{r}}{ds}\right|^2\right] \qquad (3)$$

in the inhomogeneous external field $\omega_\alpha(\vec{r}) = \delta\beta\mathcal{F}/\delta\rho_\alpha(\vec{r})$ which is created by a monomer interaction potential of Helfand type [52]

$$\beta\mathcal{F} = \frac{1}{\rho_b} \int d\vec{r} \{\chi\rho_A(\vec{r})\rho_B(\vec{r}) + \frac{\zeta}{2}(\rho_A + \rho_B - \rho_b)^2\}. \qquad (4)$$

The parameter $\zeta = 1/(\rho_b k_B T \kappa)$ is an inverse compressibility. The global compressibility of an athermal melt ($\epsilon = 0$) has been determined earlier [60], leading to $\zeta = 4.1$. However,

we have found in our simulations of homopolymer interfaces that the local density profiles are driven by a local compressibility which is much higher, leading to $\zeta = 1.9$ [51]. Note that most quantities depend only very slightly on ζ. We shall use $\zeta = 1.9$ in the following. The single chain partition function for homopolymers ($j = A, B$) and copolymers ($j = C$) is then given by the path integral

$$\mathcal{Q}_j = \int \mathcal{D}\{\vec{r}(\cdot)\}\mathcal{P}\{\vec{r}(\cdot)\}\exp\left[-\int_0^N \sum_{\alpha=A,B} ds\,\omega_\alpha(\vec{r}(s))\gamma_{\alpha,j}(s)\right], \tag{5}$$

where $\gamma_{\alpha,j}(s) = 1$ if site s on a polymer is occupied by an α monomer, and 0 otherwise. (In copolymers, for example, $\gamma_{A,C}(s) = 1$ for $s \in [0 : N/2]$, and $\gamma_{B,C}(s) = 1$ for $s \in [N/2 : N]$.) The relative density of copolymer monomers is adjusted with the parameter $\delta\mu$

$$\rho_\alpha = -\sum_{j=A,B}\frac{\delta\mathcal{Q}_j}{\delta\omega_\alpha(\vec{r})} - e^{\delta\mu}\frac{\delta\mathcal{Q}_C}{\delta\omega_\alpha(\vec{r})}. \tag{6}$$

After having solved the set of equations (4), (5) and (6) self-consistently, the interfacial tension is evaluated according to

$$\sigma = -\frac{1}{\rho_b}\int_{-\infty}^{\infty}dz\left\{\chi[\rho_A\rho_B - \rho_b^2(1-m_b^2)/4] + \frac{\zeta}{2}[(\rho_A+\rho_B)^2 - \rho_b{}^2]\right\}, \tag{7}$$

where m_b is the bulk value of the order parameter of demixing, $m = (\rho_A - \rho_B)/(\rho_A + \rho_B)$. In the following lengths shall often be given in units of $w_{\mathrm{SSL}} = b/\sqrt{6\chi}$ which is the width predicted by the self-consistent field theory in the limit of an incompressible binary mixture of infinitely long homopolymers [52].

Fig. 2 shows the bulk copolymer concentration $\rho_{b,C}$ in the two phase region as a function of the copolymer chemical potential $\delta\mu$ [23]. In the limit of small copolymer concentrations, the latter should be well approximated by

$$\delta\mu = \ln(\rho_{b,C}/\rho_b) + \chi N/2, \tag{8}$$

where the first term accounts for the translational entropy of the copolymer, and the loss of translational entropy for the homopolymers, and the second term describes for the enthalpic repulsion between homopolymers and copolymers. Fig. 2a, however, illustrates that eqn. (8) does not describe the simulation data very well. On the other hand, excellent agreement can by reached if one assumes that the value of χ for copolymer/homopolymer interactions differs from that for homopolymer/homopolymer interactions. The best fit value for $\epsilon = 0.1$ is $\chi_{cop} = 0.48$ or alternatively (using eqn. (1)) $z_{\mathrm{eff,cop}} = 2.42$. We have measured the copolymer contact number in the bulk phase and indeed found $z_{\mathrm{eff,cop}} = 2.3 \pm 0.1$ (cf. Fig. 10b). The difference to the average homopolymer contact number ($z_{\mathrm{eff}} = 2.71$) is probably caused by a difference of conformations of minority blocks and majority blocks in the homopolymer bulk phase. Earlier investigations have shown that the radius of gyration of homopolymer coils in their minority phase is reduced [61–64]. Likewise, the minority blocks in the copolymers shrink to some extent which implies that they have fewer interchain contacts at the expense of loosing some conformational entropy [63,64]. Similar effects have recently been reported experimentally [25,65].

One could now argue that consequently, different values of χ should be used for copolymer/homopolymer interactions and homopolymer/homopolymer interactions in the self-consistent field formalism. However, z_{eff} varies strongly in the interfacial region, reaching

5

values as high as $z_{\text{eff}} = 3$ in the wings of the profiles (cf. Fig. 10b). This strong position dependence cannot be derived self-consistently within our simple formulation of the theory. Hence we abide by the most idealizing approximations, taking $z_{\text{eff}} = 2.71$ independent of monomer type and position.

The area density of excess copolymers ν at the interface as a function of $\delta\mu$ is shown in Fig. 3

$$\nu = \frac{n_C - \rho_{b,c}L^2D/N}{L^2}. \tag{9}$$

The results compare quite well with the self-consistent field prediction. The extent of overlap between copolymers is reflected by the quantity $\delta A = n_C \pi R_g^2/L^2$. In the most dilute system $\delta\mu = 0$, we obtain $\delta A = 0.65$, i.e., the copolymers do not overlap. In the system with the highest copolymer concentration ($\delta\mu = 3$), the copolymers overlap strongly, $\delta A = 3.8$.

III. RESULTS

A. Interfacial width and interfacial tension

Fig. 4 shows various monomer density profiles in the dilute mushroom regime ($\delta\mu = 0$) and at the highest copolymer concentration before phase separation sets in ($\delta\mu = 3$). For comparison, the A and B profiles of pure homopolymer phases (from Ref. [51]) are also included. In the dilute case, the total profiles of A or B monomers are not affected by the presence of the copolymers [49]. In the dense case, they broaden significantly, growing from $w = 1.1w_{\text{SSL}}$ to $w = 1.5w_{\text{SSL}}$ in units of $w_{\text{SSL}} = b/\sqrt{6\chi}$. Even wider is the total interfacial region. The width of the segregation profiles of copolymers is roughly $6w_{\text{SSL}}$ at chain lengths $N = 32$, i.e., 1.5 times the radius of gyration. As discussed in the introduction, this is the width which actually determines the number of interface-strengthening entanglements. Even at the highest densities, the homopolymers are never fully expelled from the interfacial region. Thus the dry brush limit is never reached, the formation of the lamellar phase sets in in the regime where the copolymers still aggregate into a wet brush.

The individual segment profiles of end monomers of type A, $\rho_{e,A}$, of A monomers in the middle of the A block $\rho_{1/4,A}$ and of A monomers in the chain middle $\rho_{1/2,A}$ are compared to the average over all bonds in Figure 5. Each distribution is normalized to unit area. As expected, the copolymer joint profiles $\rho_{1/2,A}$ is centered around the middle of the interface, and the further one moves towards the end of the chains, the deeper the corresponding segment profile reaches into the A phase. The profile over the monomers in the block middle reproduces quite closely the average over all bonds. The agreement with the self consistent field predictions for the shape of the individual segment distributions is very good.

Now the interfacial width can be defined in different ways:

a) From a fit of the total order parameter profile $m(z) = [\rho_A(z) - \rho_B(z)]/\rho(z)$ to a tanh function: $m(z) = m_b \tanh(z/w)$.

b) From a fit of the copolymer joint profile to a Gaussian distribution $\rho_{1/2,i} \propto \exp(-\pi z^2/w_c^2)$, with $i = $ A or B [66].

6

c) From the excess internal energy e_s at the interface *via* $w_e = 2e_s/(\rho_b \chi m_b{}^2)$ [23].

Fig. 6 shows the results obtained with these different methods. The width of the copolymer joint profile follows the intrinsic width w of the AB profiles closely, but is larger by a constant factor of approximately 1.85. The estimate w_e is reasonably close to w. Also shown is the apparent width $w(B = L)$ obtained at block size $B = L = 128$. It grows much faster than w with increasing copolymer density which is a direct consequence of the fact that the interfacial tension decreases rapidly and capillary waves become more and more important for the width of the apparent profile.

This is illustrated in more detail in Figs. 7 and 8. Fig. 7 shows for different copolymer concentrations the interfacial width w in units of w_{SSL}, as obtained from a block analysis as a function of block size B. As one would expect from Fig. 6, the width grows faster with B for large copolymer concentration. The effect can be used to extract the interfacial tension from the simulation data [49]. In order to do so, however, one needs to discuss the effect of the bending stiffness on the capillary wave fluctuations which also increases with increasing copolymer content. Let $h(x, y)$ denote the local position of the interface. The capillary wave Hamiltonian then reads [67]

$$\beta \mathcal{F} = \int dx \, dy \left\{ \frac{\sigma}{2} |\nabla h(x, y)|^2 + \frac{\kappa}{2} |\Delta h(x, y)|^2 \right\}, \tag{10}$$

where σ is the interfacial tension, and κ the bending rigidity. From this expression one derives the thermal distribution of interface positions

$$P(z) = \langle \delta(z - h(x, y)) \rangle = \frac{1}{2\pi s^2} \exp(-z^2/2s^2) \tag{11}$$

$$\text{with} \qquad s^2 = \frac{1}{4\pi\sigma} \ln \left(\frac{\kappa + q_{min}^{-2}\sigma}{\kappa + q_{max}^{-2}\sigma} \right), \tag{12}$$

where the lower cutoff for blocks of size B is given by $q_{min} = 2\pi/B$, and the upper cutoff refers to the internal coarse graining length B_0, namely $q_{max} = 2\pi/B_0$. The description is of course only valid for block sizes $B > B_0$. In that case, one can approximate apparent profiles $\rho(z)$ by the convolution of intrinsic profiles $\rho_0(z)$ with the height distribution $P(z)$ (11). We have used this expression to analyze the curves in Fig. 7. It turns out that the effect of the bending rigidity on the interfacial width is quite small, $\kappa < 0.1$ for all curves, and that it may safely be neglected. Eqn. (12) with $\kappa = 0$ was then used to extract the interfacial tension. The results are shown in Fig. 8. The interfacial tension decreases to 25 % of its original value before phase separation sets in. The values are in good agreement with independent values obtained from bulk simulations by means of histogram reweighting techniques in Ref. [23].

The compatibilizing copolymers also affect the total density profile. At pure homopolymer interfaces, it exhibits a pronounced dip at the center of the interface, since reducing the total density is one (relatively expensive) way to reduce the number of unfavorable contacts there. When copolymers are added, the dip of the total density becomes smaller. Homopolymers, on the other hand, are more and more expelled from the interfacial region (Fig. 9).

B. Contact numbers and orientational properties

When looking at the contact number profiles, we recover the trends reported in our earlier study of the mushroom regime [47]. According to the usual mean field assumption, the number of self contacts should scale like $N_{\text{self}} \propto \rho$ and the number of interchain contacts like $N_{\text{inter}} \propto \rho^2$, $i.e.$, the effective coordination number is approximated by $z_{\text{eff}} \propto \rho$ independent of the monomer and chain type. Fig. 10 shows the deviations from this ideal behavior.

It turns out that homopolymer and copolymer contact numbers differ markedly from each other. The strongest position dependence is found for copolymers. The relative number of interchain contacts is reduced at the center of the interface and enhanced at distances of up to one end-to-end radius from the interface. This is because the copolymers at this distance are still in contact with the interface, and get pulled towards it by the end which sticks into the opposite phase. As a consequence, they stretch and offer more contact area. The number of self contacts decreases accordingly (Fig. 2). The profiles are thus governed by two different length scales – the interfacial width and the radius of gyration of the copolymers. At higher copolymer concentration, these effects are still present, but mellowed. The copolymers are less compact at the center of the interface than dilute copolymers, and less stretched in the wings. Qualitatively, the contact number profiles of copolymers are similar in the mushroom regime and in the brush regime.

In the case of homopolymers, the contact number profiles change qualitatively as the copolymer concentration increases. In the mushroom regime, they reflect only one length scale, the interfacial width. The effective coordination number decreases in the interfacial region (cf. Refs. [47,68]), and the number of self contacts increases. Note the fine structure at the center of the interface. It is also found in pure homopolymer interfaces and has been discussed in Ref. [51]. At higher copolymer concentrations, the contact number profiles show the signature of a second length scale which is presumably the copolymer radius of gyration. Copolymer and homopolymer profiles now influence each other. The total net excess of N_{self}/ρ and the negative excess of N_{inter}/ρ^2, however, hardly depend on the copolymer concentration.

The total number of AB contacts per monomer depends only very little on the copolymer concentration (Fig. 11). The advantage of adding copolymers is that they reduce the number of AB contacts between $homo$polymers, as shown in Fig. 12.

Finally, we discuss the effect of copolymer overlapping on the orientational properties of the copolymers and homopolymers. The squared end-to-end vector components parallel (x, y) and perpendicular (z) to the interface are shown for homopolymers and copolymers in Fig. 13 and compared to self consistent field predictions. Fig. 14 shows for comparison the same quantities for single copolymer blocks, $R_{b,ee,i}{}^2$. It is found that homopolymer coils close to the interface align to the interface, but not to the same extent in the copolymer rich regime than in the dilute regime. Likewise, the orientational tendencies of single copolymer blocks at the interface and away from the interface become weaker. It is interesting to note that copolymer blocks centered right at the interface still have a slightly parallel orientation. However, the number of blocks centered at some distance from the interface, where the average orientation is perpendicular, is now much larger. The average value of $\langle R_{b,ee}{}^2 \rangle$ at the interface with the highest possible copolymer density, $\delta\mu = 3$, is $\langle R_{b,ee,z}{}^2 \rangle = 20.0$ in the direction perpendicular to the interface, as opposed to $\langle R_{b,ee,x}{}^2 \rangle = 15.4$ in the direction parallel to the interface. Hence the net orientation is perpendicular. Note that the copolymer

8

blocks are on average slightly stretched. For comparison, we give the corresponding values in the dilute case ($\delta\mu = 0$): $\langle R_{b,ee,z}{}^2 \rangle = 17$ and $\langle R_{b,ee,x}{}^2 \rangle = 16$, *i.e.*, the copolymer blocks are hardly stretched or oriented at all.

When looking at the end-to-end vector of whole copolymers, one the additional effect comes into play, that the different blocks arrange themselves such that they stick into their majority phase. Thus molecules as a whole are orientated perpendicularly at all copolymer concentrations. However, in the dilute case, the orientation almost disappears for copolymers centered at the middle of the interface. In the dense case, it is close to constant over a region of several radii of gyration's width (Fig. 13).

IV. CONCLUSIONS

In summary, we have presented results of a large scale Monte Carlo simulation aimed towards an understanding of the modification of local structure of an interface between immiscible homopolymers due to the presence of copolymers. We have restricted ourselves to symmetric AB copolymers, comprising the same type of monomers as the corresponding homopolymers. Moreover all polymer species have identical degree of polymerization. Extending previous simulations [47] on this ternary melt we complement our knowledge of the phase diagram [23] and thermodynamical properties with a detailed analysis of the local structure of the interface at high segregation. The simulation results cover a broad range of concentrations ranging from the very dilute regime (mushroom regime) to the wet brush regime. In the latter the copolymers crowd at the interface and reduce the concentration of homopolymers at the center. However, the copolymers stretch only slightly and before we reach the dry brush regime, where the copolymers stretch significantly and the homopolymer density vanishes at the center of the interface, we encounter a first order transition to a lamellar, copolymer rich phase. This is in agreement with SCF calculations [22] and experimental studies [24,25]. To reach the dry brush regime we presumably have to increase the segregation still further and increase the chain length of the homopolymers with respect to the copolymer.

Upon increasing the copolymer concentration in the bulk phases, the areal density of amphiphilic molecules adsorbed at the interface increases. The presence of the copolymers reduces the interfacial tension and increases the width of the composition profile. The broadening of the apparent interfacial profile in the Monte Carlo simulation is due to an enhancement of capillary waves caused by the reduction of the interfacial tension, and to the increase of the width of the "intrinsic" interfacial profile. The broadening of the apparent profiles has been investigated in detail by analyzing the interfacial profiles on different lateral coarse graining length scales B. This analysis yields an estimate of the interfacial tension which agrees well with independently measured values and shows that the bending rigidity of the interface remains quite small for the chain length investigated even at rather high areal density of copolymers. Choosing the lateral coarse graining length B such that the width of the composition profile of the pure homopolymer interface agrees with its value in the SCF calculations, we have extracted "intrinsic" properties of the interfacial profiles. This procedure allows us to distinguish between the effect of capillary waves and modification of the "intrinsic" interfacial properties, and we compare our simulational results to the SCF calculations without adjustable parameter.

The calculations in the framework of the Gaussian chain model capture the dependence of the interfacial properties on the copolymer concentration qualitatively and for some quantities –*e.g.* the shape of the distribution of individual segment as a function of the distance from the interface – nearly quantitative agreement is achieved. However, other quantities – like the adsorbed amount at the interface as a function of the copolymer concentration in the bulk – deviate quantitatively from the SCF predictions. At the rather low temperature studied, the system is well segregated and local composition fluctuations, which are neglected in the SCF treatment, cannot account for the deviations. Our simulation results indicate that the conformation of the molecules depends on their local environment – *e.g.*, in their minority phase, they shrink in order to reduce the number of unfavorable intermolecular contacts and exchange them for energetically favorable intermolecular contacts. This leads to an intricate interplay between molecular conformations and the distance from the interface. The orientation of the copolymer's end-to-end vector is parallel to the interface, while the individual block orient perpendicular like the homopolymer coils. Moreover, the dependence of the molecular interaction energy is investigated in detail as a function of the distance from the center of the interface. The SCF calculations capture many but not all conformational and orientational effects at the interface.

The chain length dependence of our results has not been assessed. It is an open question to which extent these conformational changes will persist in the long chain length limit. We speculate that the orientation of the chains as a whole and the dumb-bell shape or polarization of the copolymers at the interface will persist, because the entropy costs per molecule is of the order $k_B T$, hence chain length independent. This is also in agreement with recent experimental findings [65,25]. The reduction of the effective Flory-Huggins parameter of the copolymers in the bulk phases, and the concomitant deviations from the absorption isotherm, however, is caused by a shrinking of the minority block. The corresponding entropy loss per molecule increases with chain length (at χN held constant) and simulations as well as analytical calculations [63,64] of binary homopolymer blends indicate that this effect will decrease slowly with growing chain length.

[1] D.R. Paul and S. Newman, *Polymer Blends*, Academic Press, New York (1978); K. Šolc (edt.), *Polymer Compatibility and Incompatibility*, Harwood Academic Publishers, Chur (1980); D.S. Walsh, J.S. Higgins, and A. Maconnachie, *Polymer Blends and Mixtures*, Martinus Nijhoff

Publishers, Dordrecht (1985); E.L. Thomas (edt.), *Materials Science and Technology, Vol. 12: Structures and Properties of Polymers*, VCH, Weinheim (1993).

[2] K. Binder, *Adv. Polymer Sci.* **112**, 181 (1994).

[3] G. I. Tayler, *Proc. R. Soc. London*, Ser. A 138, 41 (1932).

[4] S. Wu, *Polym. Eng. Sci.* 27, 335 (1987).

[5] E. Helfand, in *Polymer Compatibility and Incompatibility*, K. Šolc edt., Harwood Academic Publishers, Chur (1980), S. 143; G.H. Fredrickson, in *Physics of Polymer Surfaces and Interfaces*, I.C. Sanchez edt., Butterworth-Heinemann, Boston (1992), S. 1.

[6] S. Wu, *Polymer Interface and Adhesion*, Marcel Dekker, New York (1982); E.J. Kramer, L.J. Norton, C.A. Dai, Y. Sha, and C.Y. Hui, *Faraday Discuss.* **98**, 31 (1994).

[7] F.S. Bates and G.H. Fredrickson, *Annu. Rev. Phys. Chem.* **41**, 25 (1990).

[8] F.S. Bates, *Science* **251**, 898 (1991).

[9] A. Ajdari and L. Leibler, *La Recherche* **22**, 732 (1991).

[10] L. Leibler, *Makromol. Chem., Macromol. Symp.* **16**, 1 (1988).

[11] A.N. Semenov, *Macromolecules* **25**, 4967 (1992).

[12] S.H. Anastasiadis, I. Gancarz, and J.T. Koberstein, *Macromolecules* **22**, 1449 (1989).

[13] T.P. Russell, S.H. Anastasiadis, A. Menelle, G.P. Felcher and S.K. Satija, *Macromolecules* **24**, 1575 (1991).

[14] R. Israels et al, *J. Chem. Phys.* **102**, 8149 (1995).

[15] U. Jorzik and B.A. Wolf, *Macromolecules* **30**, 4713 (1997).

[16] B. Löwenhaupt and G.P. Hellmann, *Colloid Polym. Sci.* **268**, 885 (1990).

[17] H. Zhao and H. Baotong, *J. Polym. Sci.* **B 36**, 85 (1998).

[18] Y. Lee and K. Char, *Macromolecules* **27**, 2603 (1994).

[19] G.T. Pickett, D. Jasnow, and A.C. Balazs, *Phys. Rev. Lett.* **77**, 671 (1996).

[20] R. Holyst and M. Schick, *J. Chem. Phys.* **96**, 7728 (1992).

[21] M.W. Matsen, *Phys. Rev. Lett.* **74**, 4225 (1995); *Macromolecules* **28**, 5765 (1995); *J. Chem. Phys.* **103**, 3268 (1995); **107**, 8110 (1997); **108**, 785 (1998).

[22] P.K. Janert and M. Schick, *Macromolecules* **30**, 137 (1997); ibid **30**, 3916 (1997).

[23] M. Müller and M. Schick, *J. Chem. Phys.* **105**, 8885 (1996).

[24] F.S.Bates, W.W. Maurer, P.M. Lipic, M.A. Hillmyr, K. Almdal, K. Mortensen, G.H. Fredrickson, and T.P. Lodge, *Phys.Rev.Lett.* **79**, 849 (1997).

[25] H.S. Jeon, J.H. Lee, and N.P. Balsara, *Phys.Rev.Lett.* **79**, 3275 (1997); *Macromolecules* **31**, 3328 (1998); *Macromolecules* **31**, 3340 (1998).

[26] C.A. Dai et al, *Phys. Rev. Lett.* **73**, 2472 (1994).

[27] C.A. Dai, E.J. Kramer, J. Washiyama, and C.Y. Hui, *Macromolecules* **29**, 7536 (1996).

[28] K.R. Shull, E.J. Kramer, T. Hadziioannou, and W. Tang, *Macromolecules* **23**, 4780 (1990).

[29] D.G. Bucknall, J.S. Higgins, and J. Penfold, *Physica* **B 180 & 181**, 468 (1992).

[30] P.F. Green and T.P. Russell, *Macromolecules* **24**, 2931 (1991).

[31] T.P. Russell et al, *Macromolecules* **24**, 1575 (1991).

[32] A.M. Mayes, T.P. Russell, S.K. Satija, and C.F. Majkrzak, *Macromolecules* **25**, 6523 (1992).

[33] A.M. Mayes et al, *Macromolecules* **26**, 1047 (1993).

[34] A. Budkowski, J. Klein, and L. Fetters, *Macromolecules* **28**, 8571 (1995).

[35] K.R. Shull, A.M. Mayes, and Thomas P. Russell, *Macromolecules* **26**, 3929 (1993).

[36] K.H. Dai, L.J. Norton, and E.J. Kramer, *Macromolecules* **27**, 1949 (1994).

[37] K.M. Hong and J. Noolandi, *Macromolecules* **14**, 727 (1981); ibid **14**, 736 (1981); ibid **16**, 1083 (1983); J. Noolandi and K.M. Hong, *Macromolecules* **15**, 482 (1982); ibid **17**, 1531 (1984).

[38] T.A. Vilgis and J. Noolandi, *Makromol. Chem., Macromol. Symp.* **16**, 225 (1988).

[39] K.R. Shull and E.J. Kramer, *Macromolecules* **23**, 4769 (1990).

[40] K.R. Shull, *Macromolecules* **25**, 2122 (1992); ibid **26**, 2346 (1993).

[41] L.B. Fischel and D.N. Theodorou, *Faraday Trans.* **91**, 2381 (1995).

[42] For recent reviews see the articles in *Monte Carlo and Molecular Dynamics Simulations in Polymer Science*, K. Binder edt., Oxford University Press, Oxford (1995); M. Müller and F. Schmid, in *Annual Reviews of Computational Physics*, D. Stauffer edt., World Scientific, Singapore (1998).

[43] T. Pan, K. Huang, A.C. Balazs, M.S. Kunz, A.M. Mayes, and T.P. Russell, *Macromolecules* **26**, 2860 (1993).

[44] Y. Wang and W.L. Mattice, *J. Chem. Phys.* **98**, 9881 (1993); Y. Wang, Y. Li, and W.L. Mattice, *J. Chem. Phys.* **99**, 4068 (1993).

[45] G. Peng, J.U. Sommer, and A. Blumen, *Phys. Rev.* **E 53**, 5509 (1996); preprint 1997.

[46] A.C. Balazs, D. Gersappe, R. Israels, and M. Fasolka, *Macromol. Theory Simul.* **4**, 585 (1995).

[47] A. Werner, F. Schmid, K. Binder, and M. Müller, *Macromolecules* **25**, 8241 (1996).

[48] W.H. Jo and S.H. Kim, *Macromolecules* **29**, 7204 (1996); S.H. Kim, W.H. Jo, and J. Kim, *Macromolecules* **29**, 6933 (1996); ibid **30**, 3910 (1997); S.H. Kim and W.H. Jo, *J. Chem. Phys.* **108**, 4267 (1998).

[49] A. Werner, F. Schmid, M. Müller, and K. Binder, *J. Chem. Phys.* **107**, 8175 (1997).

[50] M. Müller and A. Werner, *J. Chem. Phys.* **107**, 10764 (1997).

[51] A. Werner, F. Schmid, M. Müller, and K. Binder, Phys. Rev. E, in print.

[52] E. Helfand and Y. Tagami, *J. Polym. Sci., Polym. Lett.* **9**, 741 (1971); *J. Chem. Phys.* **56**, 3592 (1971); ibid **57**, 1812 (1972); E. Helfand. *J. Chem. Phys.* **62**, 999 (1975).

[53] For a recent review see F. Schmid, *Journal of physics: Condensed matter* **10**, 8105 (1998).

[54] I. Carmesin and K. Kremer, *Macromolecules* **21**, 2819 (1988); *J. Phys. (France)* **51**, 915 (1990).

[55] W. Paul, K. Binder, D.W. Heermann, and K. Kremer, *J. Phys. II (France)* **1**, 37 (1991).

[56] H.P. Deutsch and K. Binder, *Macromolecules* **25**, 6214 (1992).

[57] M. Müller and K. Binder, *Macromolecules* **28**, 1825 (1995).

[58] K. Kremer and K. Binder, *Comp. Phys. Rep.* **7**, 261 (1988).

[59] F. Schmid and M. Müller, *Macromolecules* **28**, 8639 (1995).

[60] M. Müller and W. Paul, *J. Chem. Phys.* **100**, 719 (1994).

[61] A. Sariban and K. Binder, *J. Chem. Phys.* **86**, 5859 (1987); *Macromolecules* **21**, 711 (1988).

[62] P. Cifra, E. Nies, and J. Broersma, *Macromolecules* **29**, 6634 (1996).

[63] M. Müller and M. Schick, *J.Chem.Phys.* **105**, 8282 (1996).

[64] M. Müller, Macromolecules 1998, in press.

[65] W.W. Maurer, F.S. Bates, T.P. Lodge, K. Almdal, K. Mortensen, and G.H. Fredrickson, *J. Chem. Phys.* **108**, 2989 (1998).

[66] Integrating over this function, one obtains $\int_0^z \rho_{1/2}(z')dz' \propto \mathrm{Erf}(\sqrt{\Pi}z/(2w_c))$, which resembles a $\tanh(z/w_c)$ profile at the center of the interface

[67] F. P. Buff, R. A. Lovett, and F. H. Stillinger, *Phys. Rev. Lett.* **15**, 621 (1965); J. D. Weeks, *J. Chem. Phys.* **67**, 3106 (1977); D. Bedeaux and J. D. Weeks, *J. Chem. Phys.* **82**, 972 (1985).

[68] M. Müller, K. Binder, and W. Oed, *J. Chem. Soc. Faraday Trans.* **91**, 2369 (1995).
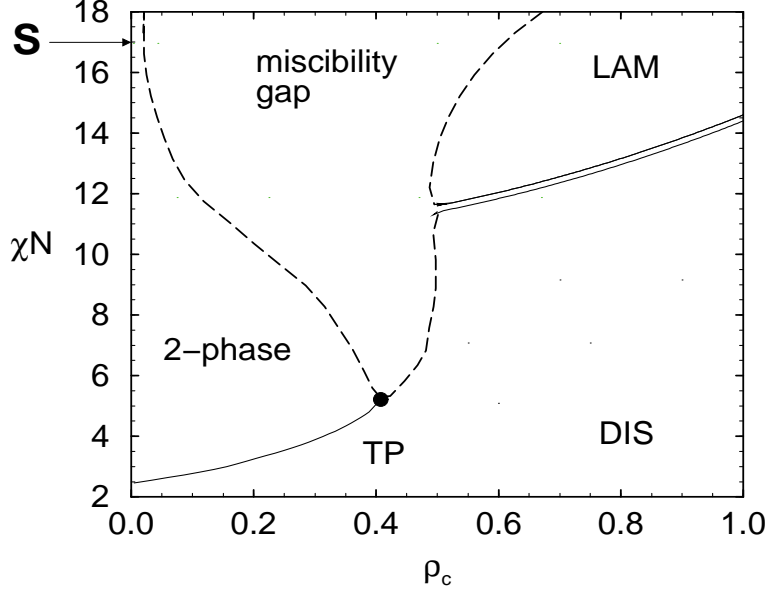
FIG. 1.

Phase diagram of a symmetric ternary mixture of A and B homopolymers and AB diblock copolymers of the same chain length $N = 32$ in the bond fluctuation model (from Ref. [23]). The exact location of the transition between the lamellar phase LAM and the disordered phase DIS has not been determined; the double solid lines are schematic. The simulations presented here were performed at $\chi N = 17$ in the two-phase region (arrow).
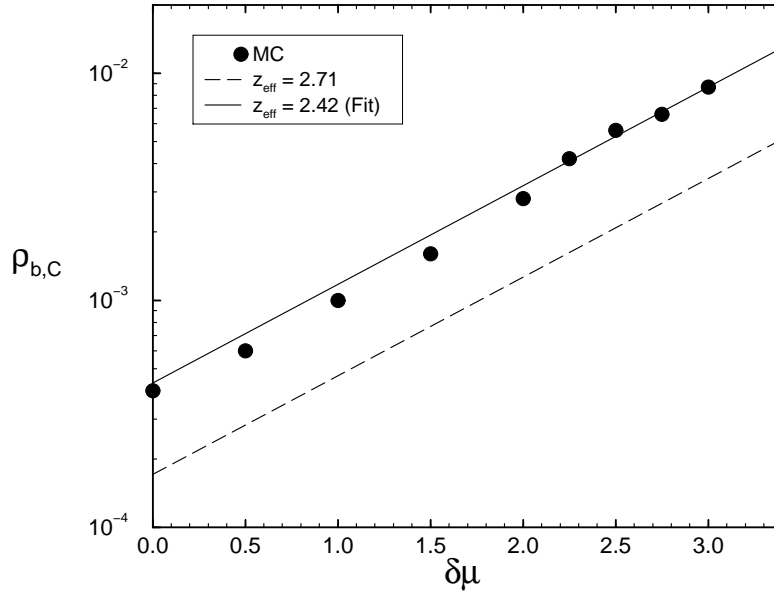

FIG. 2.

Solubility of copolymers $\rho_{b,C}$ in the homopolymer phases as a function of $\delta\mu$ at $\epsilon = 0.1$, $N = 32$ and $\Delta\mu = 0$. Symbols denote Monte Carlo results from Ref. [23]. Lines show the predictions of eqn. (8) using $z_{\mathrm{eff}} = 2.71$ (dashed) and $z_{\mathrm{eff}} = 2.42$ (solid).

14
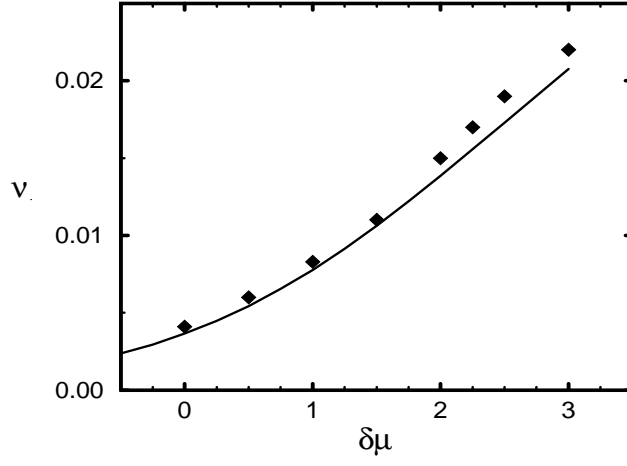
FIG. 3.

Copolymer excess ν at the interface as a function of $\delta\mu$. Solid line shows the prediction of the self-consistent field theory; filled symbols denote the Monte Carlo results from Ref. [23].

(a)
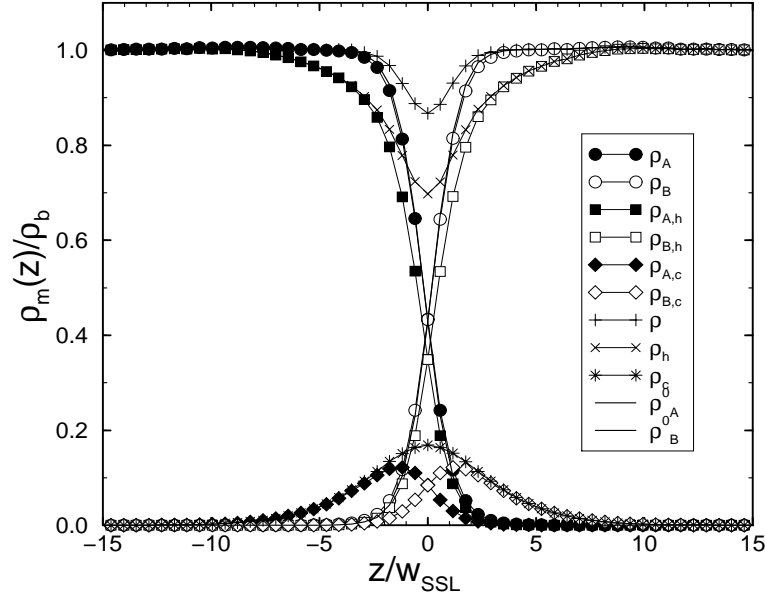
(b)
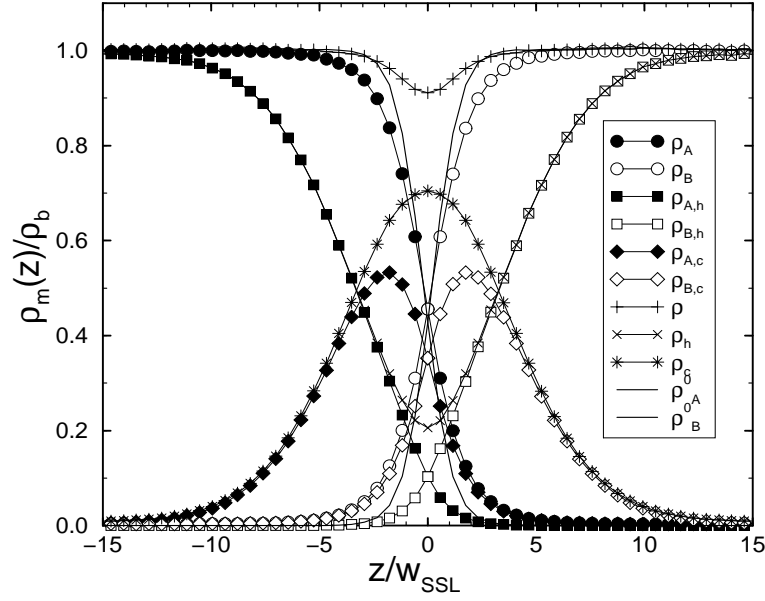
FIG. 4.

Various density profiles at (a) $\delta\mu = 0$ and (b) $\delta\mu = 3$ vs. z in units of $w_{\mathrm{SSL}} = b/\sqrt{6\chi}$. Specifically shown are the total densities of A and B monomers ρ_A and ρ_B, the densities of A and B homopolymer monomers $\rho_{A,h}$ and $\rho_{B,h}$, the densities of A and B copolymer monomers $\rho_{A,c}$ and $\rho_{B,c}$, the density of all monomers ρ, the density of homopolymer monomers ρ_h, and the density of copolymer monomers ρ_c. For comparison, the density profiles of A and B monomers ρ_A^0 and ρ_B^0 at a pure homopolymer interface are also marked. Densities are given in units of the total bulk density ρ_b.

(a)
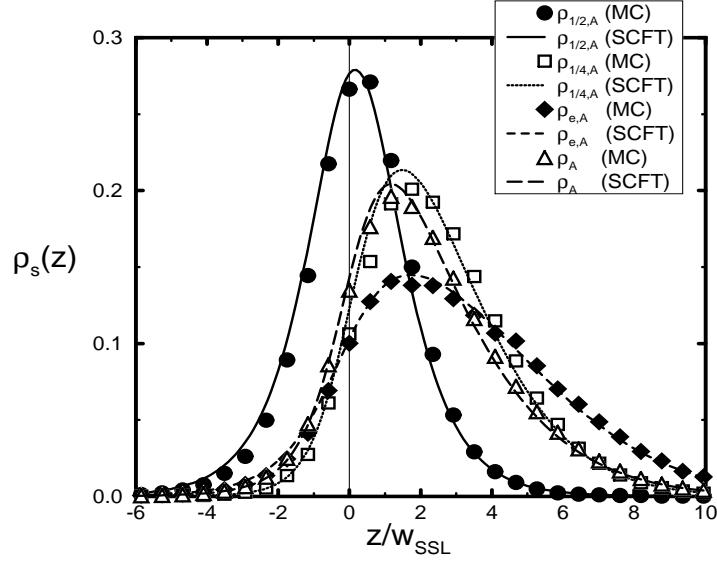
(b)
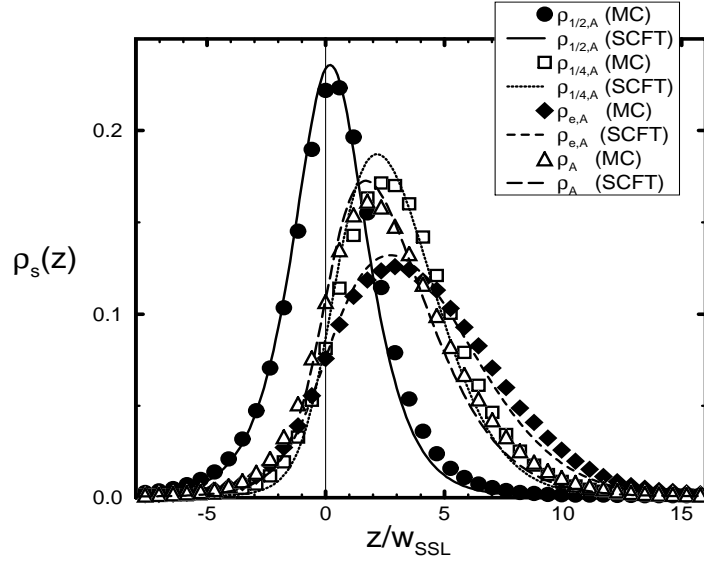
FIG. 5.

Copolymer segment profiles vs. z in units of $w_{\text{SSL}} = b/\sqrt{6\chi}$ at (a) $\delta\mu = 0$ and (b) $\delta\mu = 3$. Specifically, profiles are given for the A monomers in the middle of the chain ($\rho_{1/2,A}$), in the middle of the A block ($\rho_{1/4,A}$), and at the end of the chain (ρ_e). For comparison, the total density of A copolymer monomers is also shown (ρ_A). The lines denote the self-consistent field results. The profiles are normalized such that the area under each curve is 1.

17
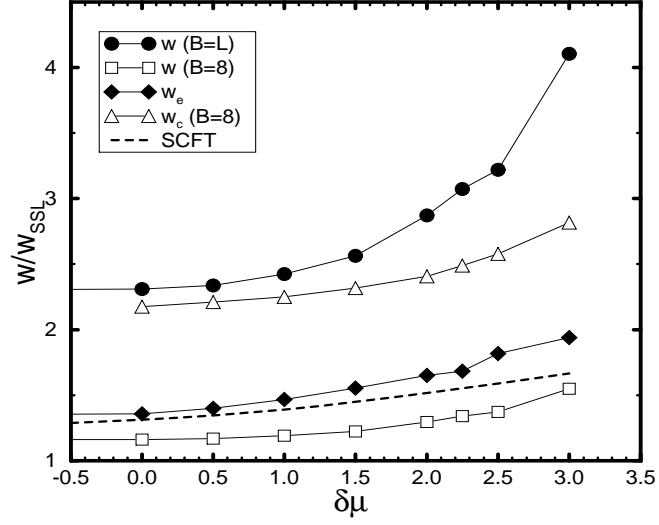
FIG. 6.

Interfacial width w in units of $w_{\mathrm{SSL}} = b/\sqrt{6\chi}$ as a function of $\delta\mu$, obtained from different definitions: From a fit of the profile $m(z)$ to a tanh profile at block size $B = L = 128$ (filled circles) and $B = 8$ (open circles), from the width of the copolymer joint profile (open triangles), and from the excess internal energy at the interface (filled diamonds, from Ref. [23]). The dashed line corresponds to the SCF calculations. See text for further explanation.
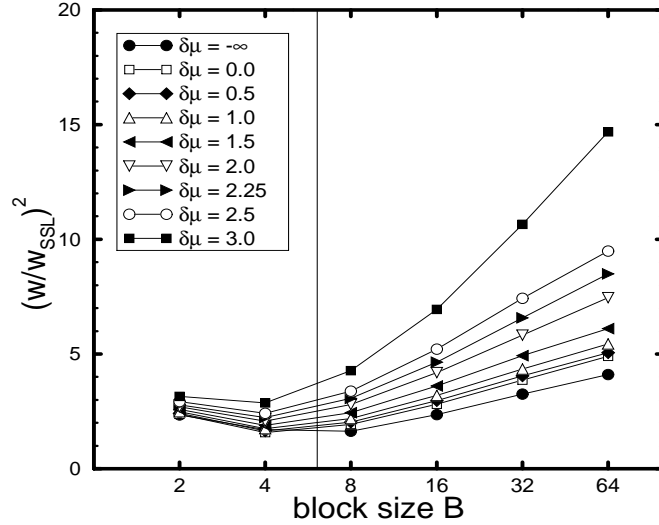
FIG. 7.

Squared interfacial width w in units of $w_{\mathrm{SSL}} = b/\sqrt{6\chi}$ as a function of block size B, obtained by fitting $m(z)$ to a tanh profile, for different values of $\delta\mu$.

18
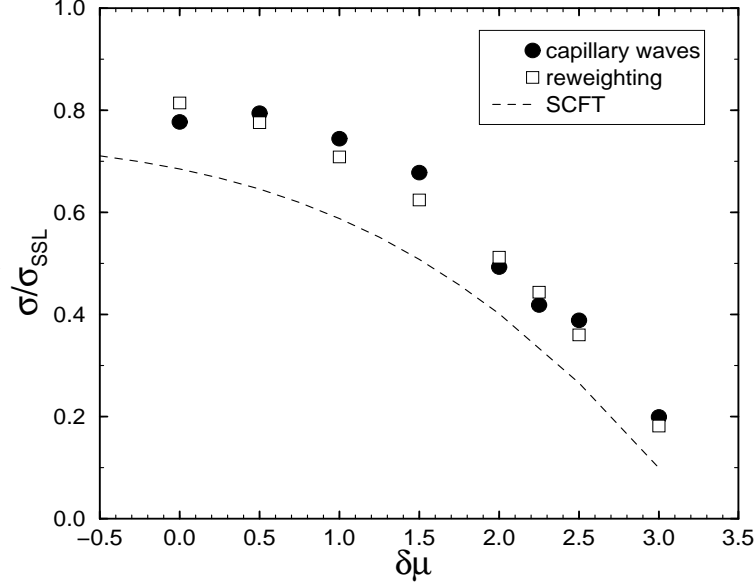
FIG. 8.

Interfacial tension σ in units of $\sigma_{\mathrm{SSL}} = \sqrt{\chi/6}\ \rho b k_B T$ as a function of $\delta\mu$. Filled circles show data obtained from the block analysis, open squares show results from Ref. [23] obtained with a histogram method, and dashed line marks the prediction of the self-consistent field theory.
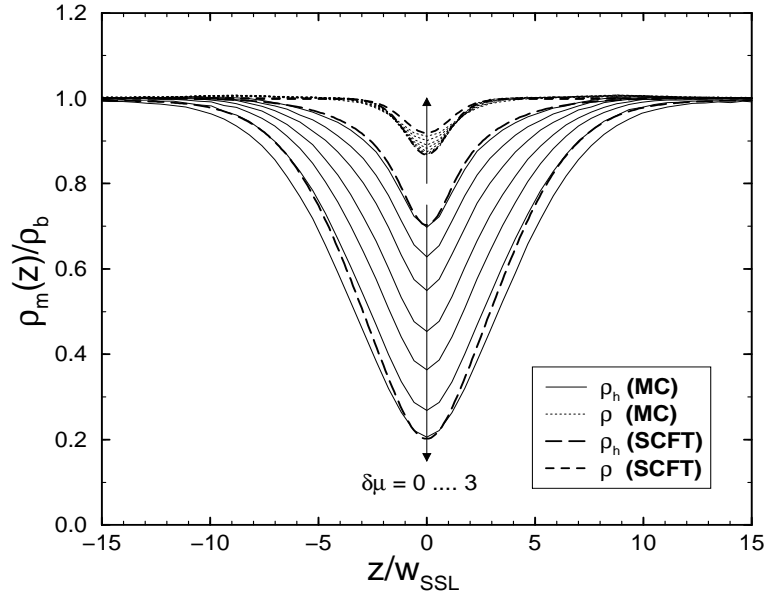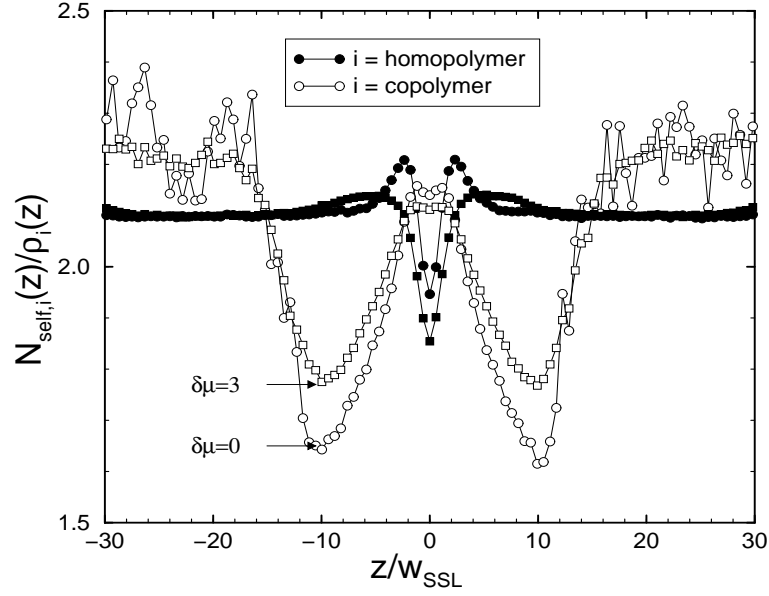

FIG. 9.

Total monomer density ρ (thin dotted lines) and homopolymer density ρ_h (thin solid lines) in units of ρ_b vs. z/w_{SSL} (with $w_{\mathrm{SSL}} = b/\sqrt{6\chi}$) for different chemical potentials $\delta\mu$ between 0 and 3 in steps of 0.5. Arrows show the direction of increasing $\delta\mu$. Thick dashed lines show the prediction of the self-consistent field theory for $\delta\mu = 0$ and $\delta\mu = 3$.
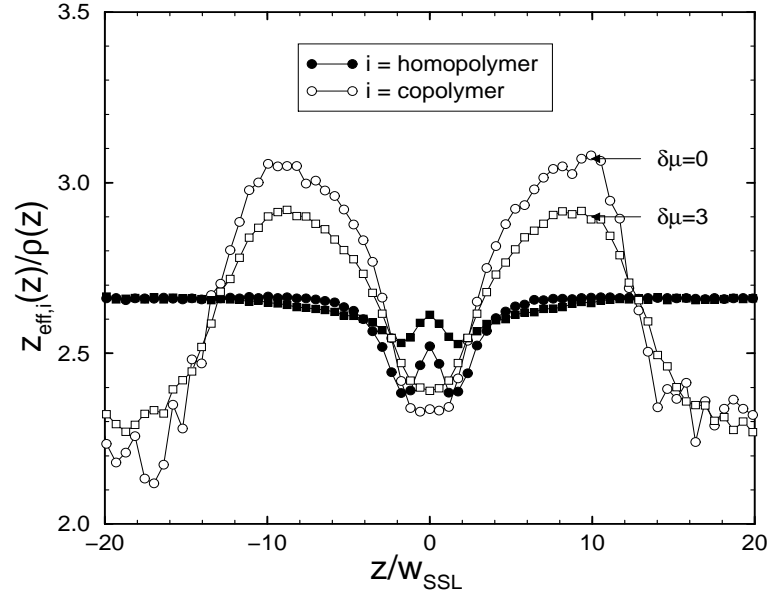
19

(a)

(b)

FIG. 10.
Normalized number of self-contacts N_{self} (a) and normalized effective coordination number z_{eff} (b) vs. z/w_{SSL} with $w_{\text{SSL}} = b/\sqrt{6\chi}$ for homopolymers and copolymers, and for $\delta\mu = 0$ and 3. Densities $\rho(z)$ are in units of ρ_b.
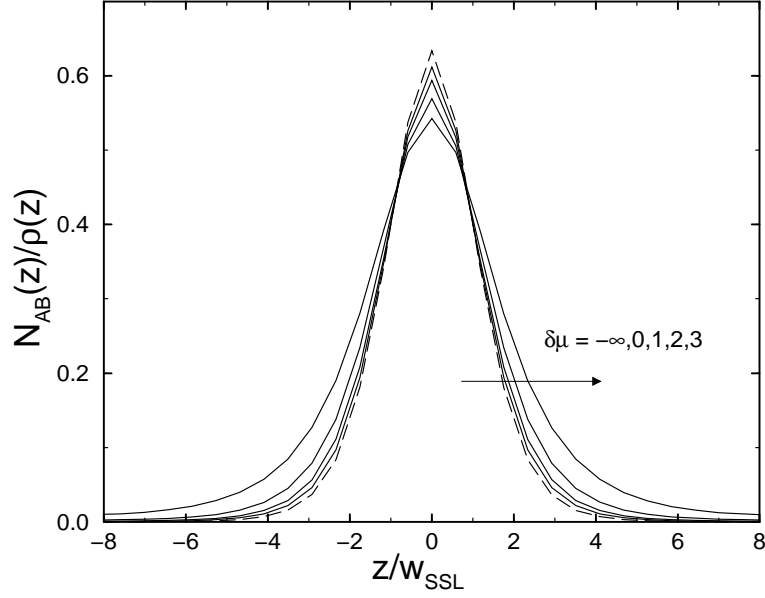
FIG. 11.

Normalized number of contacts between A and B monomers N_{AB} vs. z/w_{SSL} with $w_{\text{SSL}} = b/\sqrt{6\chi}$ for different values of $\delta\mu$, $\delta\mu \to -\infty$ and $\delta\mu \in [0,3]$ in steps of 0.5. The arrow indicates the direction of ascending $\delta\mu$. Inset shows for comparison the total number of AB contacts per monomer. Densities $\rho(z)$ are in units of ρ_b.
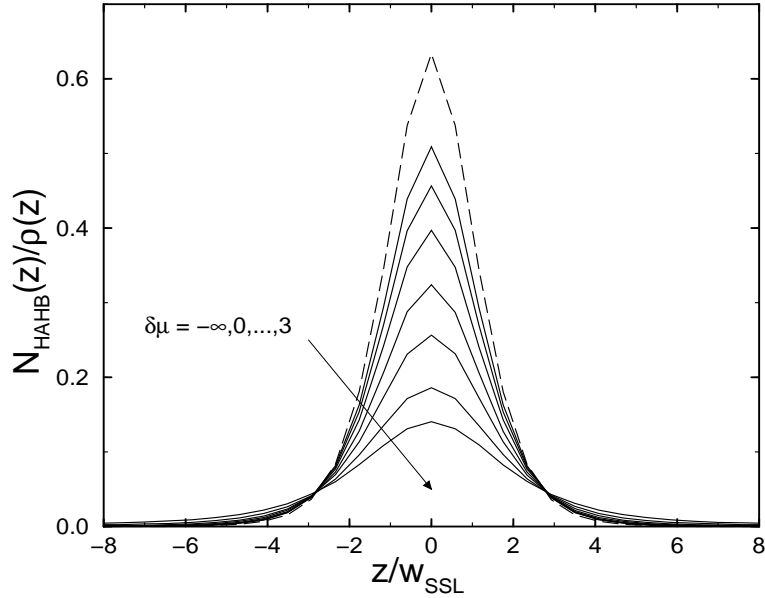

FIG. 12.

Normalized number of contacts between A and B homopolymer monomers N_{HAHB} vs. z/w_{SSL} with $w_{\text{SSL}} = b/\sqrt{6\chi}$ for $\delta\mu \to \infty$ and $\delta\mu$ between 0 and 3 in steps of 0.5. The arrow indicates the direction of ascending $\delta\mu$. Densities $\rho(z)$ are in units of ρ_b.
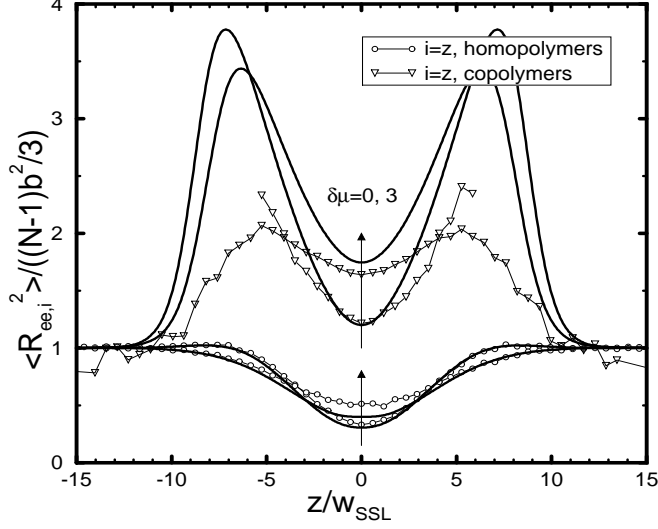
FIG. 13.

z-component of the squared end-to-end vector $R_{ee,z}^2$ in units of the bulk value, $b^2(N-1)/3$, vs. the distance z of the center of the end-to-end vector from the center of the interface in units of $w_{\mathrm{SSL}} = b/\sqrt{6\chi}$, for copolymers (triangles) and homopolymers (circles) and $\delta\mu = 0, 1, 2, 3$. Lines indicate the prediction of the self-consistent field theory for $\delta\mu = 0$ and 3.
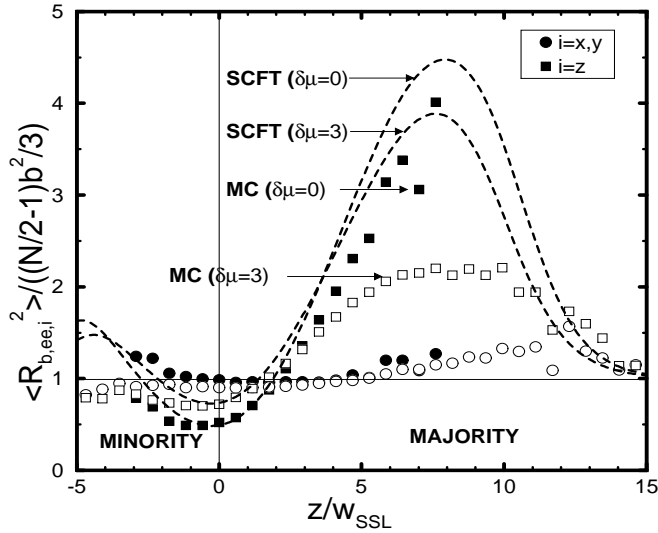

FIG. 14.

x-, y-, and z-component of the squared end-to-end vector $R_{bee,i}^2$ of the A-block in the copolymer, in units of the bulk value $b^2(N/2-1)/3$, vs. the distance z/w_{SSL} of the center of the end-to-end vector from the center of the interface, for $\delta\mu = 0$ and 3. Units are $w_{\mathrm{SSL}} = b/\sqrt{6\chi}$. Lines indicate the prediction of the self-consistent field theory.

22